Anomalous transport regime in a non-Hermitian Anderson-localized hybrid system

Himadri Sahoo,[1,2] R. Vijay,[3] and Sushil Mujumdar[1,*]
[1]Nano-optics and Mesoscopic Optics Laboratory, Tata Institute of Fundamental Research, 1 Homi Bhabha Road, Mumbai 400005, India
[2]Department of Physics and Nanotechnology, Nanophotonics Laboratory, SRM Institute of Science and Technology, Kattankulathur, Tamil Nadu 603203, India
[3]Department of Condensed Matter Physics and Materials Science, Tata Institute of Fundamental Research, 1 Homi Bhabha Road, Mumbai 400005, India

(Received 29 April 2022; revised 11 August 2022; accepted 6 September 2022; published 7 November 2022)

In a disordered environment, the average transmission of a propagating wave falls with increasing disorder. Beyond a crossover, transport is arrested because the wave is trapped in the bulk of the sample with exponentially decaying coupling to the boundaries due to Anderson localization. Here, we report the experimental demonstration of anomalous transport of hybrid particles under localizing disorder in a non-Hermitian setting. We create hybrid polariton-photon states in a one-dimensional copper sample with a comb-shaped periodic microstructure designed for microwave frequencies. Non-Hermiticity arises from multiple loss channels existing in the real experimental sample. Disorder is introduced by deliberate alterations of the periodic microstructure. Direct measurement of wave functions was achieved by a near-field probe. At a particular disorder, we observe the onset of Anderson localization of the hybrid states attested to by the exponential tails of the wave function. However, at stronger disorder and under conditions that support localization, an unexpected enhancement in the transmission was facilitated by an emergent miniband. The transmission was traced to the hopping of the hybrid particle over multiple coexisting localized resonances that exchange energy due to the nonorthogonality. These emergent states are manifested in all configurations under strong disorder, suggesting a novel transport regime. This is verified by measuring the averaged conductance which indicates an anomalous transport regime in the hybrid, non-Hermitian environment under strong disorder. These experimental observations open up new unexplored avenues in the ambit of disorder under non-Hermitian conditions.

DOI: 10.1103/PhysRevResearch.4.043081

One of the most exotic phenomena in mesoscopic physics of disorder is Anderson localization (AL), which is synonymous to quasiparticle trapping facilitated by destructive self-interference of quantum waves associated with the quasiparticle. AL occurs at the limit of strongest disorder with subsidiary regimes of transport, such as weakly localized, diffusive, quasiballistic, and ballistic manifesting with systematic reduction in disorder. Regardless of whether the quasiparticle is electronic [1,2], photonic [3–15], phononic [16], or of quantum matter [17], the degree of disorder places the transport in one of the above regimes. Of late, however, novel and unexpected behavior has been reported from non-Hermitian photonic systems that fails to justify the underlying strength of disorder [18,19].

The advent of deliberate non-Hermiticity has led to prominent developments in photonics in recent years. Engineered non-Hermitian structures have revealed a plethora of exciting photonic behaviors, such as the striking revelation of exceptional points associated with patity-time symmetry implemented through simultaneous loss and gain [20–22]. In the domain of complex systems, random lasers were the first non-Hermitian systems [23–26], although non-Hermiticity was not invoked in the physics thereof. Deliberate non-Hermiticity introduced theoretically in topological disordered lattices exhibited a gapless energy spectrum in the metallic phase, in stark contrast to the gapped spectrum in the Hermitian case [27]. Furthermore, in two-dimensional lattices, non-Hermiticity was shown to modify the level-spacing statistics [28], although it preserves the Anderson transition in three-dimensional lattices [29]. Apart from inclusion of gain (negative imaginary refractive index), systems with pure dissipation also exhibit interesting transport behavior. For instance, measurements have been carried out on diffusive and localized transport in open systems [30–32]. Such open samples have helped in identifying specific effects caused by non-Hermiticity, namely, increased eigenfunction correlation accompanied by strong modal anticorrelation that facilitates normalized transport [33]. Furthermore, the presence of non-Hermiticity erases the equivalence among total excited energy, dwell time, and density of states (DoS) that, otherwise, exists in the Hermitian system [34]. Recently, a surprising development was reported in which a localized system was shown to exhibit transport by a novel mechanism through sudden jumps between distant sites [33], a result which has also been experimentally verified [35]. Overall, one can expect

*mujumdar@tifr.res.in

non-Hermiticity to continue unraveling novel effects in quasiparticle transport in mesoscopic systems.

On a parallel note, ongoing studies in mesoscopic transport are exploring an entity of particular interest, namely, composite or hybrid quasiparticles. These particles are created in systems wherein strong interactions between two forms of energy are induced by the underlying structure. They react to a disordered environment with novel emergent behavior. For instance, novel topological phases were discovered in photon-phonon composites in cavity optomechanical systems [36], which were further shown to exhibit a nontrivial frequency dependence of localization length in a disordered environment [37]. Interestingly, Anderson localization was demonstrated to be a potential resource to enhance the coupling between phononic and photonic components to manifest strongly hybridized composites [38]. The challenges in colocalization of the two components has been overcome in cleverly designed GaAs/AlAs random superlattices [39].

Given the intricacies that non-Hermiticity and hybridization bring to mesoscopic transport, one can expect exciting consequences of simultaneous presence of both. Precisely such a scenario is addressed in this paper. We experimentally unravel a novel anomalous transport regime at localizing disorder in a hybrid non-Hermitian system. Spoof surface plasmon polaritons (SSPPs) [40] realized in a corrugated metal structure were employed as the composite particles. The SSPPs are generated due to the hybridization of the cavity resonant mode with the polariton mode. We have confirmed the occurrence of the anomalous transport regime (ATR) by measuring the generalized conductance in the disordered system. In corroboration of our earlier theoretical work, we find that the transport is effected via the manifestation of necklace states [41–49] as identified from direct measurements of phase jumps occurring in an emergent miniband at high disorder. Concomitant simulations reveal the constituent localized resonances in the measured necklace states. A statistical study of the necklace states reveals the high probability of their occurrence and, hence, the certainty of the ATR in such systems.

Our experimental samples comprise the well-established SSPP structures in the form of one-dimensional arrays of microwave resonators cast into comb-shaped corrugated metal strips as shown in Fig. 1(a). In a single unit cell of periodicity $d = 6$ mm, the groove depth and width are denoted by h and a, respectively, and the strip width and thickness are m and t, respectively Fig. 1(b). The structure is sculpted, using a commercial circuit board milling machine, onto an FR4 dielectric substrate (a commercial printed circuit board) with $\epsilon_r = 4.4$ and total thickness of 1.45 mm. Several periodic samples of metallic corrugated strips with varying h were fabricated using the milling machine and experimentally tested at designated microwave frequencies. The dissipation in our system exists due to multiple reasons. First, the metal and substrate (FR4) offer material dissipation at the relevant frequencies. Next, the input and output ports make this an open system. And finally, the unavoidable fabrication limitations create out-of-plane scattering. Although our setup does not directly measure the out-of-plane scattering, the fact that the resolution of the circuit board milling machine is limited implies that the subresolution corrugations will channel the electromagnetic energy into free space. The collective dissipation can

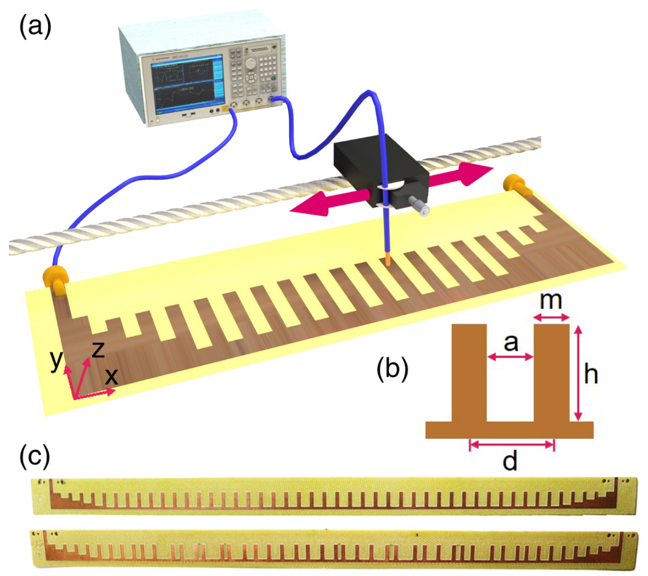

FIG. 1. Experimental setup and SSPP structure. (a) Schematic of the near-field microwave experimental setup comprising the SSPP sample and a vector network analyzer for the source and detection. (b) Unit cell of the SSPP structure with dimensions $d = 6$ mm (lattice constant); $m = 2$ mm (metal corrugation width); $h = 7$ mm (height), and $t = 35$ μm (metal film thickness). (c) Images of the fabricated samples using standard printed circuit board (PCB) fabrication technique: periodic (top) and disordered (bottom).

be quantified by the diminishing amplitude of the intensity distribution in the periodic system. Our samples exhibited a loss length of $\sim 1.84 L_{\text{sys}}$. See Supplemental Material (Sec. S2) [50] for the measurements.

Disorder is introduced into the system by randomly displacing the position of each resonator by an amount determined by a uniformly distributed random variate $\Sigma \in [-\delta a/2, \delta a/2]$, where $0 \leqslant \delta \leqslant 1$ represents the disorder strength. Multiple configurations of disordered samples with $\delta = 0.3, 0.5$ (referred to as moderate disorder, hereafter) and 0.7 and 0.9 (strong disorder) were fabricated. Figure 1(c) shows a fabricated periodic and a disordered sample. We built impedance-matching structures at the output and input ends of the array to ensure efficient launch of the microwave signal into the sample. This was accomplished by constructing metal teeth with gradually increasing heights over a few unit cells at the two ends [51]. The experimental setup consisted of an Agilent E5071C Vector Network Analyzer (VNA), an SMA connector to input the microwave signal at one end and a monopole antenna that acts as the detector. The other end was terminated with a 50-Ω resistor. The detector, attached onto an XY translation stage, is numerically controlled by a stepper motor. The sample was mounted taut horizontally such that the probe distance from the surface of the sample remained $\sim$1.5 mm at any point along the X axis (axis of translation). The scanning step was 1 mm to obtain high-resolution images. The probe picked up the complex E_z field during the scan, which was recorded by the VNA. In support of the experimental measurements, finite-element computations were carried out using the rf module of COMSOL MULTIPHYSICS software. Eigenmode analysis was carried out in the simulation for the

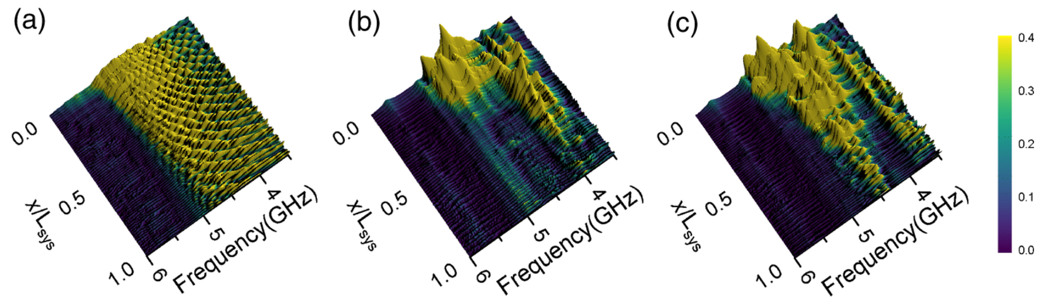

FIG. 2. Measured spatial intensity distribution $\mathbf{I}(\mathbf{x})$ maps for three structures. (a) Periodic ($\delta = 0.0$), (b) moderate disorder ($\delta = 0.5$), and (c) high disorders ($\delta = 0.7$). An isolated localized mode is seen in (b) around 4.0 GHz, a high-transmission mode close to 4.5 GHz seen in (c).

same structures as in the experiments, as well as transmission profiles were calculated by implementing a lumped port as a source of excitation.

The experimentally measured spatial distribution of intensity $I(x)$ is shown in Fig. 2. Image Fig. 2(a) represents the intensity in the periodic structure. Figures 2(b) and 2(c) show the spatial intensity for two particular configurations at moderate disorder ($\delta = 0.5$) and high disorder ($\delta = 0.7$), respectively. The sample is excited from one end at $x/L_{\mathrm{sys}} = 0$, where L_{sys} is the total system length. The spectrally resolved field is recorded at each x position at which the source signal is swept through a frequency range of 3.5 to 6 GHz. For the periodic system Fig. (2a), extended modes are formed across the system for all frequencies up to the band edge at 4.77 GHz. The band gap (beyond 4.77 GHz) is completely devoid of modes. These frequencies were in excellent agreement with the finite-element calculations as elaborated in Supplemental Material S1 [50]. Figure 2(b) shows an isolated localized mode with exponentially decaying tails on both sides at intermediate disorder $\delta = 0.5$ around ∼4 GHz. The decay length of the mode was measured to be $\sim 0.34 L_{\mathrm{sys}}$. Image Fig. 2(c) depicts the behavior at high disorder $\delta = 0.7$. Beyond 4 GHz, the transport decays substantially due to the strong disorder. Nonetheless, extended modes are observed around the frequency of 4.5 GHz despite the strong disorder, leading to high transmission. That these extended modes were of the character of necklace states was directly inferred from two diagnostics, namely, the experimentally measured phase characteristics and the computed eigenmode analysis.

The hybridization occurring in this system is a consequence of the interaction between the cavity resonant frequency ($f_c = 5.35$ GHz, dashed gray line) of the resonant cavity and the polariton line (gray solid line) as shown in Fig. 3(a). The avoided crossing due to this interaction also results in an upper branch (not shown here) of the dispersion curve which is radiative as it lies above the light line. The bound lower branch corresponds to the SSPP dispersion which occurs at a much lower frequency range compared to SPP dispersion, which in the case of copper, occurs in the petahertz range. The hybridization was experimentally verified by measuring the dispersion diagram of the finite-sized periodic and disordered structures and comparing it with the expected resonance characteristics. Figures 3(a)–3(c) show the said dispersion. The white dotted curve in Fig. 3(a) illustrates the dispersion behavior computed using the eigenmode solver of COMSOL MULTRPHYSICS after applying periodic boundary conditions. The experimental modes are in excellent agreement with the computed dispersion, confirming successful excitation of SSPPs formed over the structured metal surface. The band edge lays at 4.77 GHz. The cyan arrows indicate the width Δk at any frequency, which is inversely proportional to the spatial extent of the mode at the frequency. Figures 3(b) and 3(c) show the measured dispersion of two particular configurations at high disorder $\delta = 0.7$ and 0.9, respectively. Disorder clearly broadens the Δk at a few frequencies as labeled by the arrows, reflecting the spatial localization of modes. The violet arrows represent localized modes as inferred from the spatial studies (discussed further), whereas the cyan arrows indicate persisting extended

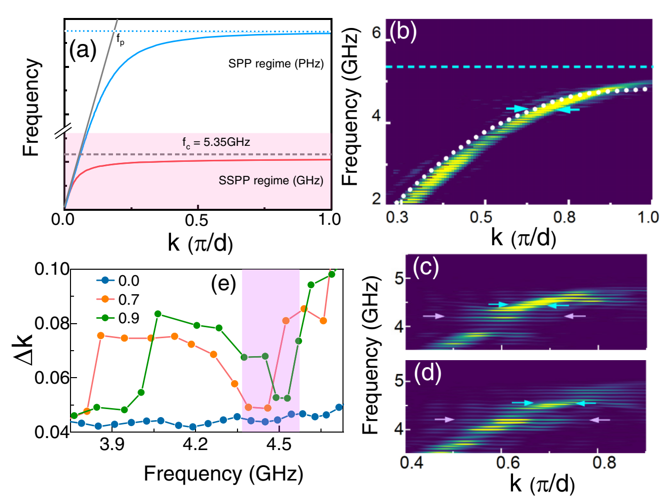

FIG. 3. (a) Theoretically computed dispersion for SSPP structures(red curve) and SPP curve for copper(blue curve). Gray dashed line marks the cavity resonant frequency($f_c = 5.35$ GHz) and the blue solid line is the plasma frequency of copper ($f_p \sim$ PHz). The break in the Y axis signifies the very low frequency of SSPP in comparison to the surface plasmon. (b) Experimentally measured dispersion for the finite SSPP structures. Dashed cyan line: Nondispersive resonant mode (5.35 GHz) for an infinite sample. Dotted white curve: Hybrid mode at the band edge ∼4.77 GHz. Measured experimental results (Viridis color map) show the hybrid band in excellent agreement with the predicted band. Arrows demarcate the FWHM of the k-space peaks. Highly disordered structures: (c) $\delta = 0.7$ and (d) $\delta = 0.9$. (e) Δk as a function of frequency, measured at the three values of disorder. The band-edge region (vertical purple band) shows a drop in Δk.

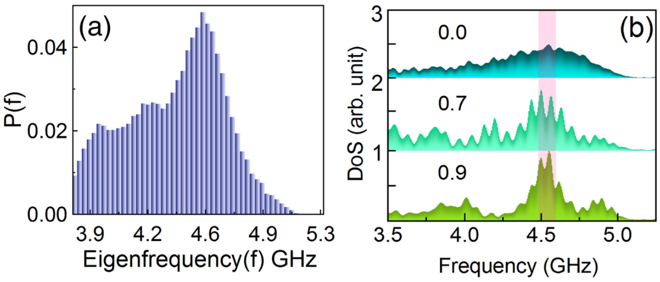

FIG. 4. Probability distribution of eigenfrequencies for an ensemble of highly disordered configurations showing eigenfrequency condensation around the band edge (∼4.7 GHz). (b) Measured DoS as a function of frequency. The band-edge region (shaded pink) shows an enhanced DoS, a consequence of frequency pinning in hybrid systems.

states in the structure even under strong disorder. The coexistence of localized and extended states is revealed in subplot of Fig. 3(d), which illustrates the systematic variation of Δk with frequency. Blue circles represent the periodic structure, with narrow and almost uniform Δk across the frequency axis. Orange and green circles ($\delta = 0.7$ and 0.9, respectively) illustrate a rise in the Δk at frequencies where localization sets in. Both curves show a fall in the shaded frequency region where the extended states manifest.

Unlike conventional dielectric systems, in a hybrid plasmonic system under high disorder, the eigenvalues cannot migrate deep into the band gap. They tend to accumulate in the vicinity of the band edge and the hybridization region. Our simulations detected this behavior in the eigenvalues as discussed in Fig. 4, which shows the frequency pinning in hybrid plasmonic systems [18]. Interestingly, we note that a similar phenomenon called "eigenvalue condensation" was theoretically observed for strong randomness in imaginary potentials [33]. The non-Hermiticity lifts the orthogonality of the pinned eigenmodes and enables energy transport between them. In this scenario, whenever multiple localized eigenmodes overlap even minimally in the tails, the energy can be transmitted through the chain of eigenmodes, that is, the so-formed necklace states (see Supplemental Material S5) [50]. Theoretically, it is expected that these extended states formed by the pinning lie in an emergent miniband. In the experimental data, as illustrated in (b), such a miniband can be directly inferred from the increased DoS shown in the same frequency (shaded) region. In the weak disorder limit ($\delta = 0.0$, 0.3), the DoS shows a typical behavior where it consistently increases up to the band edge. The miniband manifests at $\delta = 0.7$ and is strongly conspicuous at $\delta = 0.9$.

The necklace states, essentially coupled localized resonances, can be analyzed by observing the phase jumps in the constituent phase profile [45] measured from complex field at the output end of the samples. Every component resonance effects a phase shift of π. Figure 5 discusses the phase behavior of a particular necklace state observed in a sample with high disorder. The green curve depicts the measured transmission spectrum (left Y axis). The peak at around 3.7 GHz represents the photonic bands wherein localization has not yet set in. The drop in transmission at ∼4 GHz represents incipient localization. Next, a broad anomalous peak is seen in the

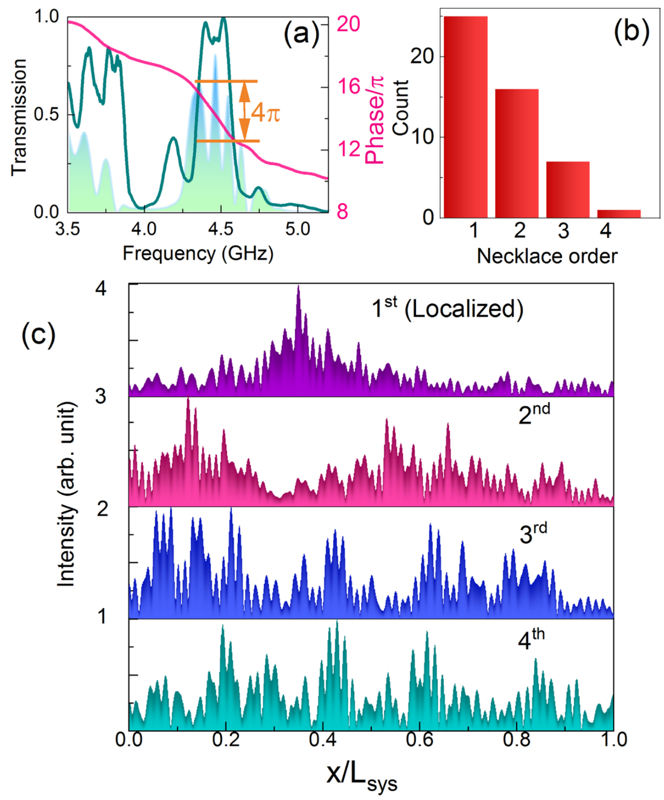

FIG. 5. Measurement of phase and necklace state order in samples with high disorder. (a) Experimentally measured transmission spectrum (green solid line) and the corresponding extracted phase (pink solid line) for a single configuration at high disorder. A drop in phase by a magnitude of 4π endorses a fourth order necklace state. The simulated transmission spectrum (shaded green) is in excellent agreement with the experimental measurements and indeed reveal four resonances in the necklace (see Supplemental Material S3) [50]. (c) shows the necklace order m distribution measured over 49 modes. (c) Spatial intensity distributions measured for different orders of necklace states.

vicinity of the band edge at around 4.5 GHz which represents the miniband formed due to the coalescence of eigenvalues. The peak at ∼4.2 GHz is not a consequence of the structure, as ascertained from various configurations. The phase, as extracted from the complex E_z measurement, is shown in the pink curve (right Y axis). A clear jump of 4π is observed over the frequency range pertinent to the miniband. Corresponding simulations for this particular disorder configuration provided the theoretical transmission spectrum shown by the overlapping shaded green region. Eigenvalue analysis of this spectrum clearly revealed four constituent coupled resonances creating the necklace state. See Supplemental Material S3 [50] for details. Over the measured 49 states in 21 samples, the distribution of localized modes and necklace states is shown in the bar graph in Fig. 5(b). The measured phase jump of 4π endorses this coupling. Several such necklace states of various orders were observed, and a few representative states are shown in Fig. 5(c). The top panel shows an order 1, i.e, essentially a conventional Anderson localized mode [see Fig. 2(b)] with a localization length $\xi/L_{\text{sys}} = 0.3$. The lower panels exhibit necklace states with orders 2–4, respectively,

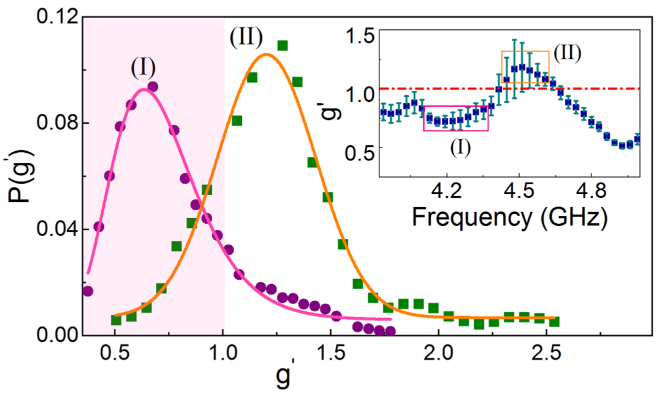

FIG. 6. Effect of disorder on generalized conductance. The inset: Measured $\langle g' \rangle$ from intensity distributions averaged over 21 configurations as a function of frequency. The pink shaded regime up to $\langle g' \rangle = 1$ demarcates localization regime. Main plot: $P(g')$ measured at two regions as marked by pink and orange rectangles in (a): (I) localized region ($\langle g' \rangle < 1$): long-tailed distribution, best fit with a log-normal function (solid line) with mean $\langle g' \rangle = 0.6$ and width $\sigma_g = 0.07$. (II) Anomalous transmission regime ($\langle g' \rangle \geqslant 1$): The distribution exhibits a Gaussian profile with mean $\langle g' \rangle = 1.2$ and width $\sigma_g = 0.2$.

as characterized by the measured phase jumps. As seen, almost 50% localized states couple to form necklace states of some order. This fact distinguishes the hybrid non-Hermitian system from conventional systems wherein the necklace states are statistically rare and do not contribute to average transport. In contrast, the high probability of necklace states in this system induces anomalous transport. It is interesting to note how dissipation acts differently in coupled eigenmodes in localized and diffusive systems. In a diffusive system, the transport occurs due to weak quasimodes that are already strongly coupled [52]. The weakness of the quasimodes arises from the coupling to the boundaries. In this situation, any absorption merely reduces the amplitude of all quasimodes and, hence, the overall transmission. In contrast, in the localizing system, the native quasimodes are quite strong and are weakly coupled to each other. Here, the dissipation succeeds in coupling the quasimodes and enhancing transmission, although the associated decay in amplitude also exists in this case.

The average transmission in disordered systems can be characterized by a parameter known as the generalized conductance g', derived from the intensity fluctuations. The g' can faithfully characterize localization even in dissipative systems [7]. When a sample is in the localized regime, the value of g' turns out to be below unity. Our samples are designed to be in the localized regime, and yet we see extended states therein, which indicates a novel regime of transport. In order to confirm the regime of transport uncovered in this best, we calculate the generalized conductance of the samples in the presence of the necklace states as shown in Fig. 6. The g' is provided by $2/3\text{var}(I)$, where I is either the normalized total transmission, or in-plane spatial intensity in a one-dimensional sample [7,53]. We extracted the generalized conductance $\langle g' \rangle$ over 21 highly disordered configurations. Figure 6(a) shows the average generalized conductance $\langle g' \rangle$ vs frequency, with $\langle g' \rangle = 1$ delimiting the onset of the Anderson localized regime. In the vicinity of 4.5 GHz, the $\langle g' \rangle$ is clearly seen to rise above 1, endorsing the anomalous transport. The error bars indicate the standard deviation of the g' values indicating that the majority of the samples were close to, or in the anomalous transport regime. For lower frequencies, $\langle g' \rangle < 1$ for the localized regime. The distribution of conductance $P(g')$ follows a stipulated behavior in disordered systems. The rectangles (I) and (II) in the inset of six demarcate the regions over which g' values were chosen to create the $P(g')$, shown in the main Fig. 6. In the localized regime [magenta dots from rectangle (I)], the distribution is asymmetric and long-tailed, and nicely fit by a log-normal function with mean 0.6 as seen from solid the magenta curve. That conductances in the localized regime are distributed log-normally is a well-established fact also confirmed experimentally [8,14,15]. On the other hand, in the ATR [green squares, data from rectangle (II)], the distribution is symmetric albeit with a longer tail. The data are excellently fit by a Gaussian distribution as is expected in the metallic regime. The mean $\langle g' \rangle = 1.2$ from the Gaussian fit.

These data lie at the boundary of localization-delocalization. For this regime, we apply the theory established in Ref. [54], where the authors theoretically examine the conductance distributions in one-dimensional disordered systems. In a particular situation where localized and extended states coexist, the $P(g')$ for the metallic states is shown to follow a Gaussian function $P(g') \propto \exp[-\frac{15}{2}(g' - \langle g' \rangle)^2]$. Clearly, the experimental data in Fig. 6 shows an excellent fit to this equation, which provides a value of $\langle g' \rangle = 1.16$, whereas the experimental value was measured to be 1.2, once again in excellent agreement. These data conclusively endorse the existence of the system in a properly conducting regime, despite insulating disorder. The insulating nature of disorder is certified by the fact that, at frequencies away from the band edge where necklaces are not yet forged, the conductances are consistently subunity. The probability distributions $[P(I/\langle I \rangle)]$ of normalized intensity measured at localized, and the necklace state regimes are provided in Supplemental Material S4 [50]. We note here that very similar behavior was reported earlier in conventional localizing samples wherein the crossover ($g' \sim 1$) was achieved by weakening the disorder [8]. In our samples, the crossover occurred at the same strong disorder, aided by the necklace states.

In conclusion, we have successfully uncovered an anomalous transport regime in hybrid non-Hermitian systems. One-dimensional structures supporting spoof surface plasmon polaritons were investigated for the same. Conventional Anderson localization leading to arrested transport was observed at moderate disorders. However, at high disorder, an enhancement in transmission is facilitated by formation of necklace states. The hitherto reported necklace states in localizing systems are rare [2]. In contrast, in the hybrid non-Hermitian system, the necklace states manifest persistently for all configurations at high disorder. The anomalous transmission manifests in the vicinity of the band-edge frequency where frequency pinning of modes occurs due to constrained migration. The resulting emergent miniband has been experimentally demonstrated in our experiments. Direct mode mapping using a near-field spatial probe allowed us to image the necklace states as well as identify the order thereof via phase jumps.

The latter provided a direct measure of the component localized modes within the state, which was in excellent agreement with our numerical calculations on the various configurations. The transport regime is labeled via the measurement of generalized conductance $\langle g' \rangle$, which was consistently above 1, endorsing high transmission even under localizing conditions. Comparing the distribution of g' with theoretical expressions for one-dimensional disordered systems close to the localization transition, we found that our system was indeed in a "metallic" state despite the strong disorder.

ACKNOWLEDGMENTS

We thank M. Balasubrahmaniyam and K. C. Joshi for useful discussions and helpful comments. We thank M. Patankar for his help in sample making. We acknowledge funding from the Department of Atomic Energy, Government of India (Grants No. 12-R and No. D-TFR-5.02-0200). S. Mujumdar acknowledges the Swarnajayanti Fellowship from the Department of Science and Technology, Government of India.

[1] P. W. Anderson, Absence of diffusion in certain random lattices, Phys. Rev. **109**, 1492 (1958).
[2] J. B. Pendry, Quasi-extended electron states in strongly disordered systems, J. Phys. C **20**, 733 (1987).
[3] D. S. Wiersma, P. Bartolini, A. Lagendijk, and R. Righini, Localization of light in a disordered medium, Nature (London) **390**, 671 (1997); *see also* F. Scheffold, R. Lenke, R. Tweer, and G. Maret, Localization or classical diffusion of light? Nature **398**, 206 (1999); *see also* D. S. Wiersma, J. G. Rivas, P. Bartolini, A. Lagendijk, and R. Righini, *ibid.* **398**, 207 (1999).
[4] M. Segev, Y. Silberberg, and D. N. Christodoulides, Anderson localization of light, Nat. Photonics **7**, 197 (2013).
[5] P. D. García, S. Stobbe, I. Söllner, and P. Lodahl, Nonuniversal Intensity Correlations in a Two-Dimensional Anderson-Localizing Random Medium, Phys. Rev. Lett. **109**, 253902 (2012).
[6] D. S. Wiersma, Disordered photonics, Nat. Photonics **7**, 188 (2013).
[7] A. A. Chabanov, M. Stoytchev, and A. Z. Genack, Statistical signatures of photon localization, Nature (London) **404**, 850 (2000).
[8] Z. Shi, J. Wang, and A. Z. Genack, Microwave conductance in random waveguides in the cross-over to Anderson localization and single-parameter scaling, Proc. Natl. Acad. Sci. USA **111**, 2926 (2014).
[9] S. E. Skipetrov and I. M. Sokolov, Absence of Anderson Localization of Light in a Random Ensemble of Point Scatterers, Phys. Rev. Lett. **112**, 023905 (2014).
[10] A. Z. Genack and N. Garcia, Observation of Photon Localization in a Three-Dimensional Disordered System, Phys. Rev. Lett. **66**, 2064 (1991).
[11] A. Yamilov, S. E. Skipetrov, T. W. Hughes, M. Minkov, Z. Yu, and H. Cao, Anderson localization of electromagnetic waves in three dimensions, arXiv:2203.02842.
[12] S. Smolka, Quantum correlations and light localization in disordered nanophotonic structures, Ph.D. thesis, 2010.
[13] S. Pandey, B. Gupta, S. Mujumdar, and A. Nahata, Direct observation of Anderson localization in plasmonic terahertz devices, Light Sci. Appl. **6**, e16232 (2017).
[14] R. Kumar, S. Mondal, M. Balasubrahmaniyam, M. Kamp, and S. Mujumdar, Discrepant transport characteristics under Anderson localization at the two limits of disorder, Phys. Rev. B **102**, 220202(R) (2020).
[15] S. Mondal, R. Kumar, M. Kamp, and S. Mujumdar, Optical Thouless conductance and level-spacing statistics in two-dimensional Anderson localizing systems, Phys. Rev. B **100**, 060201(R) (2019).
[16] H. Hu, A. Strybulevych, J. H. Page, S. E. Skipetrov, and B. A. van Tiggelen, Localization of ultrasound in a three-dimensional elastic network, Nat. Phys. **4**, 945 (2008).
[17] J. Billy, V. Josse, Z. Zuo, A. Bernard, B. Hambrecht, P. Lugan, D. Clément, L. Sanchez-Palencia, P. Bouyer, and A. Aspect, Direct observation of Anderson localization of matter waves in a controlled disorder, Nature (London) **453**, 891 (2008).
[18] M. Balasubrahmaniyam, A. Nahata, and S. Mujumdar, Anderson localization at the hybridization gap in a plasmonic system, Phys. Rev. B **98**, 024202 (2018).
[19] M. Balasubrahmaniyam, S. Mondal, and S. Mujumdar, Necklace-State-Mediated Anomalous Enhancement of Transport in Anderson-Localized non-Hermitian Hybrid Systems, Phys. Rev. Lett. **124**, 123901 (2020).
[20] L. Feng, R. El-Ganainy, and L. Ge, Non-Hermitian photonics based on parity–time symmetry, Nat. Photonics **11**, 752 (2017).
[21] S. Longhi, Parity-time symmetry meets photonics: A new twist in non-Hermitian optics, Europhys. Lett. **120**, 64001 (2017).
[22] M.-A. Miri and A. Alú, Exceptional points in optics and photonics, Science **363**, eaar7709 (2019).
[23] D. S. Wiersma, The physics and applications of random lasers, Nat. Phys. **4**, 359 (2008).
[24] H. Cao, Y. G. Zhao, S. T. Ho, E. W. Seelig, Q. H. Wang, and R. P. H. Chang, Random Laser Action in Semiconductor Powder, Phys. Rev. Lett. **82**, 2278 (1999).
[25] H. Cao, Review on latest developments in random lasers with coherent feedback, J. Phys. A **38**, 10497 (2005).
[26] S. Mujumdar, M. Ricci, R. Torre, and D. S. Wiersma, Amplified Extended Modes in Random Lasers, Phys. Rev. Lett. **93**, 053903 (2004).
[27] J. M. Zeuner, M. C. Rechtsman, Y. Plotnik, Y. Lumer, S. Nolte, M. S. Rudner, M. Segev, and A. Szameit, Observation of a Topological Transition in the Bulk of a Non-Hermitian System, Phys. Rev. Lett. **115**, 040402 (2015).
[28] A. F. Tzortzakakis, K. G. Makris, and E. N. Economou, Non-Hermitian disorder in two-dimensional optical lattices, Phys. Rev. B **101**, 014202 (2020).
[29] Y. Huang and B. I. Shklovskii, Anderson transition in three-dimensional systems with non-Hermitian disorder, Phys. Rev. B **101**, 014204 (2020).
[30] J. Wang and A. Z. Genack, Transport through modes in random media, Nature (London) **471**, 345 (2011).
[31] M. Davy and A. Z. Genack, Selectively exciting quasi-normal modes in open disordered systems, Nat. Commun. **9**, 4714 (2018).

[32] P. Sebbah, B. Hu, J. M. Klosner, and A. Z. Genack, Extended Quasimodes within Nominally Localized Random Waveguides, Phys. Rev. Lett. **96**, 183902 (2006).

[33] A. F. Tzortzakakis, K. G. Makris, A. Szameit, and E. N. Economou, Transport and spectral features in non-Hermitian open systems, Phys. Rev. Res. **3**, 013208 (2021).

[34] Y. Huang, Y. Kang, and A. Z. Genack, Wave excitation and dynamics in non-Hermitian disordered systems, Phys. Rev. Res. **4**, 013102 (2022).

[35] S. Weidemann, M. Kremer, S. Longhi, and A. Szameit, Non-Hermitian Anderson Transport arXiv:2007.00294.

[36] V. Peano, C. Brendel, M. Schmidt, and F. Marquardt, Topological Phases of Sound and Light, Phys. Rev. X **5**, 031011 (2015).

[37] T. F. Roque, V. Peano, O. M. Yevtushenko, and F. Marquardt, Anderson localization of composite excitations in disordered optomechanical arrays, New J. Phys. **19**, 013006 (2017).

[38] P. D. García, R. Bericat-Vadell, G. Arregui, D. Navarro-Urrios, M. Colombano, F. Alzina, and C. M. Sotomayor-Torres, Optomechanical coupling in the Anderson-localization regime, Phys. Rev. B **95**, 115129 (2017).

[39] G. Arregui, N. D. Lanzillotti-Kimura, C. M. Sotomayor-Torres, and P. D. García, Anderson Photon-Phonon Colocalization in Certain Random Superlattices, Phys. Rev. Lett. **122**, 043903 (2019).

[40] X. Shen, T. J. Cui, D. Martin-Cano, and F. J. Garcia-Vidal, Conformal surface plasmons propagating on ultrathin and flexible films, Proc. Natl. Acad. Sci. USA **110**, 40 (2013).

[41] L. Chen, W. Li, and X. Jiang, Occurrence probability and conductance contribution of necklace states: In support of a new scenario of Anderson phase transition, New J. Phys. **13**, 053046 (2011).

[42] L. Chen and X. Jiang, Characterization of short necklace states in the logarithmic transmission spectra of localized systems, J. Phys.: Condens. Matter **25**, 175901 (2013).

[43] M. Ghulinyan, Formation of optimal-order necklace modes in one-dimensional random photonic superlattices, Phys. Rev. A **76**, 013822 (2007).

[44] J. Bertolotti, S. Gottardo, D. S. Wiersma, M. Ghulinyan, and L. Pavesi, Optical Necklace States in Anderson Localized 1D Systems, Phys. Rev. Lett. **94**, 113903 (2005).

[45] J. Bertolotti, M. Galli, R. Sapienza, M. Ghulinyan, S. Gottardo, L. C. Andreani, L. Pavesi, and D. S. Wiersma, Wave transport in random systems: Multiple resonance character of necklace modes and their statistical behavior, Phys. Rev. E **74**, 035602(R) (2006).

[46] C. Wang and X. R. Wang, Level statistics of extended states in random non-Hermitian Hamiltonians, Phys. Rev. B **101**, 165114 (2020).

[47] S. H. Choi, K. M. Byun, and Y. L. Kim, Excitation of multiple resonances in 1D Anderson localized systems for efficient light amplification, Opt. Lett. **40**, 847 (2015).

[48] F. Sgrignuoli, G. Mazzamuto, N. Caselli, F. Intonti, F. S. Cataliotti, M. Gurioli, and C. Toninelli, Necklace state hallmark in disordered 2D photonic systems, ACS Photonics **2**, 1636 (2015).

[49] K. Y. Bliokh, Y. P. Bliokh, V. Freilikher, A. Z. Genack, and P. Sebbah, Coupling and Level Repulsion in the Localized Regime: From Isolated to Quasiextended Modes, Phys. Rev. Lett. **101**, 133901 (2008).

[50] See Supplemental Material at http://link.aps.org/supplemental/10.1103/PhysRevResearch.4.043081 for details about band formation in SSPP structures, material loss in SSPP structures, eigenmodes corresponding to phase jumps atATR, measured probability distribution of intensity in localized and ATR, and necklace state confirmation through eigenmodes.

[51] X. Gao, L. Zhou, Z. Liao, H. F. Ma, and T. J. Cui, An ultra-wideband surface plasmonic filter in microwave frequency, Appl. Phys. Lett. **104**, 191603 (2014).

[52] A. Z. Genack and S. Zhang, *Chapter 9: Wave Interference and Modes in Random Media, Tutorials in Complex Photonic Media*, edited by M. A. Noginov, G. Dewar, M. W. McCall, and N. I. Zheludev (SPIE, 2009).

[53] K. Joshi, S. Mondal, R. Kumar, and S. Mujumdar, Reduction in generalized conductance with increasing gain in amplifying Anderson-localized systems, Opt. Lett. **45**, 2239 (2020).

[54] K. Muttalib, P. Wölfle, and V. A. Gopar, Conductance distribution in quasi-one-dimensional disordered quantum wires, Ann. Phys. (NY) **308**, 156 (2003).